VOL. 6, NO. 8, AUGUST 2011 ISSN 1819-6608
ARPN Journal of Engineering and Applied Sciences

www.arpnjournals.com

MIXED CONVECTIVE HEAT TRANSFER IN RECTANGULAR ENCLOSURES FILLED WITH POROUS MEDIA

M. A. Waheed[1], G. A. Odewole[2] and S. O. Alagbe[3]
[1]Department of Mechanical Engineering, College of Engineering, University of Agriculture, Abeokuta, Ogun State, Nigeria
[2]School of Mechanical, Aerospace and Civil Engineering, The University of Manchester, United Kingdom
[3]Department of Offshore, Process and Energy Resources, School of Engineering, Cranfield University, United Kingdom
E-Mail: s.o.alagbe@cranfield.ac.uk

ABSTRACT

The mixed convective heat transfer in a fluid-saturated porous medium has been investigated numerically using the generalized non-Darcy model. The problem governing equations including the continuity, the generalized Darcy-Brinkman-Forchheimer extended momentum and the energy transport equations were thereby solved using the finite difference method. The flow governing parameters including the Darcy, Richardson and Péclet numbers, and the length-to-height aspect ratio were varied in the range $10^{-3} \le Da \le 10$, $0.1 \le Ri \le 10$, $1 \le Pe \le 10^3$ and $0.5 \le AR \le 4$ respectively while the Reynolds number was held constant at a value of $Re = 100$ for all computations. The results are presented in the form of the streamlines and isotherms contours, and the profiles for horizontal component of velocity, temperature and the local heat flux. The results show that all the flow governing parameters have strong influence on the flow pattern and heat distribution within the enclosure.

Keywords: mixed convection, heat transfer, porous media, buoyancy, stream function, isotherms, finite difference scheme.

INTRODUCTION

Fluid flow and heat transfer by mixed convection in which the effect of shear- and the buoyancy-driven flow are in comparable magnitude, occurs in many industrial, engineering and scientific practices. The problem involved has been extensively studied in the past few decades due to the numerous areas of applications in the clear and porous media. Some of the few areas of practical applications of the mixed convective heat transfer in clear media include cooling of electronic systems, thermal-hydraulics of nuclear reactors, thermal convection in micropolar fluids, chemical processing equipment, and lubricating grooves. Other areas of applications are in crystal growing, materials processing such as float glass production, galvanizing, metal coating, drying and casting technologies, food processing, and industrial processes where a solid ribbon or a solid material is heated as it moves through a furnace, improvement of performance of heat exchangers and so on [1 - 7]. The study of heat and mass transfer by natural convection in porous media has gained prominence over the years due to its important applications in such areas as geothermal energy and reservoir engineering, chemical reactors engineering, insulation of buildings, equipment and pipes, and the storage of grains and the heat generating materials such as coal, regenerative heat exchangers containing porous materials, heat extraction from geothermal fields, the disposal of hazardous waste in subsurface salt formations, and the modelling of convection in the underground storage of CO_2, flushing out of contaminants, oil or heat from various types of porous medium and so on [8 - 11]. The understanding of the flow mechanism due to the interactions between the natural and forced convection heat transfer in porous media in many of the practical applications highlighted above is essential for the enhanced design and characterization of these systems.

Many of the works that have been done on the convection heat transfer in rectangular fluid-saturated porous enclosures is based on the Darcy's law. This model is, however, not valid for many practical engineering applications since it only gives good approximation for low-porosity media, and does not account for no-slip boundary condition and the inertia effects. The inclusion of more physical realism in the Darcian fluid model is therefore very important for the accurate modelling of any practical problem [12]. The study of the heat and mass transfer by mixed convection has been carried out by the extension of the Darcy's law leading to such models as Darcy - Brinkman and Darcy - Brinkman - Forchheimer model [8, 13 - 15]. A comprehensive review of the theoretical, numerical and experimental works carried out on convection heat transfer in porous media can be found in the monograph by Nield and Bejan [16].

In a numerical study of the free and forced convection in porous media, Holzbecher and Yusa [17] applied the Darcy's law for fluid flow and the Fourier's law for heat transport. Different flow phenomena were captured based on the interaction of the flow and heat transfer. Khanafer and Chamkha [15] applied the extended Darcy equation for flow in the porous media in their numerical study of the mixed convection in a stratified fluid-saturated porous medium by incorporating the convection term in the model. The effects of the Darcy, Richardson and the internal Rayleigh number on the flow and thermal field were thereby investigated. Abdelkhalek [18] extended the work of Khanafer and Chamkha [15] by solving the extended Darcy equation through the perturbation technique. There are good agreements between the results presented by these two different research groups. Al-Amiri [13] studied the effect of the Darcy and Richardson number on the characteristics of the fluid flow and temperature fields in a stable thermal-

stratified two-dimensional square cavity filled with a water-saturated porous medium. The generalized Darcy-Brinkman-Forchheimer model, which incorporated the inertia and viscous terms in the momentum equations, was used in the numerical study. The results show that the inertia effects retard the momentum and energy transport especially at higher values of the Darcy number or lower values of the Richardson number. Khanafer and Vafai [14] carried out the numerical investigation of the double-diffusive mixed convection in a lid-driven enclosure filled with fluid-saturated porous medium. Their findings show that the Richardson number and higher negative values of the buoyancy ratio enhance the heat transfer and flow characteristics inside the cavity while these are suppressed by higher values of the Lewis number. In another parallel study, Jue [19] studied the effect of torsional oscillatory lid-driven flow on the hydrodynamic and thermal field in a fluid-saturated porous enclosure with thermal stable stratification. The results show that the influence of the oscillatory frequency is so serious in heat flux variation at some particular frequency corresponding to the resonant frequency. The parameter $Gr/(Re^2\,Da)$ was found to have importance on the flow such that an increase in its value retards the stable stratification from the top surface and extend to the interior domain. In all the cases reviewed above, the heating is done on the upper wall while cooling is from below. In the numerical analysis carried out by Oztop [20] on the combined convection heat transfer on the top lid-driven porous enclosure partially heated on the side and cooled on the moving lid, the lower and the right vertical walls are thermally isolated. The generalized Darcy-Brinkman-Forchheimer model was applied. The results indicate that the heat transfer, which decreases with increase in the Richardson number and increases with increase in the Darcy number, is optimum when the heater is located on the left vertical wall.

Most of the previous studies on mixed convection in fluid-saturated porous enclosures are based on the upper lid-driven stable stratified flow in which the enclosure is heated on the upper horizontal wall while being cooled from below. While many different boundary conditions are present in practice to capture and characterize the effects of the flow governing parameters on the mixed convection and heat transfer mechanism in many practical applications, flow configuration close to physically real practical cases with more complex boundary conditions should be studied. This is what motivates this work. The subject of this work is therefore to study the mixed convective heat transfer in porous media contained in a rectangular enclosure that is being cooled from the lower, upper and left vertical walls. The right vertical wall of the enclosure is thermally isolated and the shear and buoyancy flow is induced by a heated lid that moves through the enclosure at the mid-horizontal plane at uniform speed as shown in Figure-1. The principal objective of this work is to investigate the influence of the flow governing parameters including the Richardson, Darcy and Péclet numbers, and the aspect ratio on the flow characteristics, energy distribution and heat transfer behaviour for this configuration.

THE PHYSICAL AND MATHEMATICAL MODELS

Consider a continuously moving horizontal plate emerging from a slot at a uniform velocity U_w and at temperature T_w into an enclosure of height, H, and length, L, filled with fluid-saturated porous medium. The plate divides the rectangular enclosure into two equal halves as shown in Figure-1.

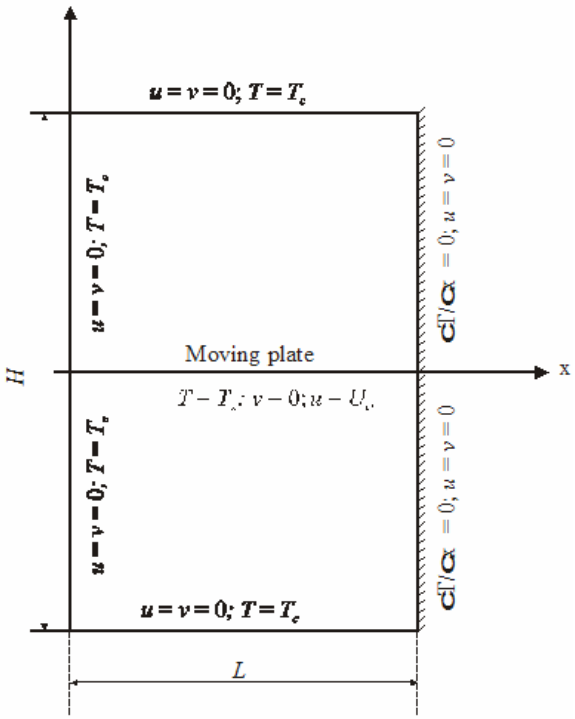

Figure-1. Schematic representation of the physical problem with the boundary constraints and the coordinate axes.

The enclosure is bounded by a thermally isolated wall on the right vertical side, and isothermal walls at temperature T_c, respectively on the lower, upper and on the left vertical side, where temperature T_c is lower than the temperature of the moving plate ($T_c < T_w$). Consequently, the heat transfer process characterised by the combined effects of the buoyancy- and shear-driven convection ensues in the enclosure. The enclosed fluid is assumed to be Newtonian and incompressible, and the fluid flow is single-phase, steady, two-dimensional, laminar and non-Darcian. All the physical and transport properties of the fluid are assumed invariable but for the density variation in the buoyancy term for which the Oberbeck-Boussinesq approximation is used [16]. The volumetric body force is thereby defined as the product of the density and the acceleration due to gravity:

$$\rho f_j = \rho_\infty \left(1 - \beta\left(T - T_\infty\right)\right) g \qquad (1)$$

The no-slip boundary conditions are adopted for velocities on the walls consequent upon which the

horizontal and vertical velocity components are set to zero on the stationary walls and to the specified velocity on the moving plate. The porous matrix is assumed to be rigid, made of spherical particles, hydrodynamic and thermally isotropic, homogeneous and in local thermal equilibrium with the fluid with which it is saturated. It was further assumed that the heat transfer by radiation, the internal heat generation and the viscous-energy-dissipation are negligible.

The balance laws for the conservation of mass, linear momentum and thermal energy based on the local volume-averaged approach govern the flow and heat transfer processes in the system. The momentum equations are thereby expressed in the generalized Darcy-Brinkman-Forchheimer model. The governing equations are stated here in indicial notation form valid for all coordinate systems, fluid and flow types [14, 21]:

Continuity equation:

$$\frac{\partial \rho}{\partial t} + \frac{\partial}{\partial x_i}\left(\rho u_i\right) = 0 \tag{2}$$

Momentum equations:

$$\frac{\partial}{\partial t}\left(\frac{\rho u_i}{\varepsilon}\right) + \frac{\partial}{\partial x_i}\left(\rho u_i \frac{u_j}{\varepsilon^2}\right) = - \frac{\partial p}{\partial x_j} + \frac{\partial}{\partial x_i}\left(\frac{\mu_e}{\varepsilon}\frac{\partial u_j}{\partial x_i}\right) - \left(F\frac{\rho}{\sqrt{K}}|\boldsymbol{u}| + \frac{\mu}{K}\right)u_j + \rho f_j \tag{3}$$

Energy equation:

$$\left(\rho c_p\right)_e \frac{\partial T}{\partial t} + \left(\rho c_p\right)_f u_i \frac{\partial T}{\partial x_i} = \frac{\partial}{\partial x_i}\left(k_e \frac{\partial T}{\partial x_i}\right). \tag{4}$$

where,

$$\left(\rho c_p\right)_e = \varepsilon\left(\rho c_p\right)_f + \left(1-\varepsilon\right)\left(\rho c_p\right)_s$$

$$k_e = \varepsilon k_f + \left(1-\varepsilon\right)k_s$$

Here c_p denotes the specific heat capacity at constant pressure, t the time, T the temperature, u_i the fluid velocity components, respectively in the directions x_i (i = 1, 2, 3 in 3-D problem), p the average pressure read of the gauge and the subscripts f and s, respectively stand for fluid and solid. The physical properties in the above equations include the fluid density ρ, the fluid dynamic viscosity μ, the effective viscosity μ_e, the permeability K, the Forchheimer coefficient, also known as the form-drag term F, the porosity ε and k the thermal conductivity. Other parameters are ρf_j the volumetric body force in the j direction, g the acceleration due to gravity, and β the volumetric coefficient of thermal expansion. While the physical parameters including the fluid density ρ, the fluid dynamic viscosity μ, and the porosity ε can be measured independently; the other three, namely the effective viscosity μ_e, the permeability K, and the Forchheimer coefficient F depend on the geometry of the permeable membrane and thus cannot be measured directly nor determined analytically due to lack of model equation relating them to basic quantities [22]. For a packed-sphere bed, the permeability and the Forchheimer coefficient are related to the porosity ε and the diameter of the solid particle, d_p, of the porous medium [10, 13]:

$$K = \frac{d_p^2 \varepsilon^3}{A\left(1-\varepsilon\right)^2} \quad \text{and} \quad F = \frac{B}{\left(150\varepsilon^3\right)^{1/2}} \tag{5}$$

where A and B are empirical constants found by Ergün [23] to be A = 150 and B = 1.75. The porosity is assumed uniform in the enclosure for which a value of 0.9 is considered in this work.

The problem is subject to the following prescribed boundary conditions:

$$u = v = 0, \quad T = 0 \text{ at } x = 0$$

$$u = v = 0, \quad \frac{\partial T}{\partial x} = 0 \text{ at } x = L$$

$$u = U_w, v = 0, \; T = T_w \text{ at } y = 0$$

$$u = v = 0, T = T_c \text{ at } y = \pm H/2 \tag{6}$$

MODEL ANALYSIS AND NUMERICAL TECHNIQUE

The flow equations (2) - (4) are simplified within the limit of the basic assumptions stated above to the expressions describing the flow and the heat transfer processes in two-dimensional Cartesian coordinates. For the purpose of the numerical solutions of these equations and the prescribed boundary conditions, the x- and the y-momentum equations are foremost reduced by eliminating the pressure gradient terms to a single equation. The resulting equation is simplified with the help of the continuity equation (2), the expressions describing the velocity components as the derivatives of the stream function,

$$u = \frac{\partial \psi}{\partial y}, \quad v = -\frac{\partial \psi}{\partial x}, \tag{7}$$

and the vorticity equation,

$$\omega = \frac{\partial v}{\partial x} - \frac{\partial u}{\partial y} \tag{8}$$

to give the vorticity transport equation in non-dimensional form [13, 14]

$$\varepsilon\frac{\partial \Omega}{\partial \tau} + U\frac{\partial \Omega}{\partial X} + V\frac{\partial \Omega}{\partial Y} = \frac{\varepsilon}{Re}\left(\frac{\partial^2 \Omega}{\partial X^2} + \frac{\partial^2 \Omega}{\partial Y^2}\right) - \frac{\varepsilon^2}{DaRe}\Omega - \frac{F\varepsilon^2}{\sqrt{Da}}|\boldsymbol{U}|\Omega +$$

$$\frac{F\varepsilon^2}{\sqrt{Da}}\left(U\frac{\partial|\mathbf{U}|}{\partial Y}-V\frac{\partial|\mathbf{U}|}{\partial X}\right)+\varepsilon^2 Ri\frac{\partial\theta}{\partial X} \quad (9)$$

and the dimensionless stream function equation describing the flow kinematics:

$$\Omega=-\left(\frac{\partial^2\Psi}{\partial X^2}+\frac{\partial^2\Psi}{\partial X^2}\right) \quad (10)$$

The energy equation (4) is also simplified and non-dimensionalized to give

$$\frac{\partial\theta}{\partial\tau}+U\frac{\partial\theta}{\partial X}+V\frac{\partial\theta}{\partial Y}=\frac{1}{RePr}\left(\frac{\partial^2\theta}{\partial X^2}+\frac{\partial^2\theta}{\partial Y^2}\right) \quad (11)$$

The above equations are reduced to dimensionless form through the introduction of the following scales:

$$X=\frac{x}{H},\quad Y=\frac{y}{H},\quad U=\frac{u}{U_w},\quad V=\frac{v}{U_w},\quad \tau=\frac{tU_w}{H}$$

$$\theta=\frac{T-T_c}{T_w-T_c},\quad \Psi=\frac{\psi}{U_wH},\quad \Omega=\frac{\omega}{U_w/H}, \quad (12)$$

where ω and ψ stand for the dimensional vorticity and stream function respectively, U_W is the plate velocity and H is the height of the enclosure.

The principal non-dimensional parameters appearing in the above equations are the Reynolds number, *Re*, the Prandtl number, *Pr*, the Darcy number, *Da*, and the Richardson number, *Ri,* which is defined as the ratio of the Grashof number, *Gr*, to the square of the Reynolds number. The product of the Reynolds and the Prandtl number gives the Péclet number, *Pe*, which is an important parameter in the study of the heat transfer by convection.

The corresponding boundary conditions in non-dimensional form are;

$$U=V=\Psi=0,\ \Omega=\left(\frac{\partial V}{\partial X}\right)_{X=0},\ \theta=0 \text{ at } X=0$$

$$U=V=\Psi=0,\ \Omega=\left(\frac{\partial V}{\partial X}\right)_{X=1},\ \frac{\partial\theta}{\partial X}=0 \text{ at } X=1$$

$$U=1, V=\Psi=0,\ \Omega=\left(\frac{\partial U}{\partial Y}\right)_{Y=0},\ \theta=1 \text{ at } Y=0$$

$$U=V=\Psi=0,\ \Omega=\left(\frac{\partial U}{\partial Y}\right)_{Y=\pm0.5},\ \theta=0 \text{ at } Y=\pm0.5 \quad (13)$$

The vorticity at the non-slip boundary is obtained by a Taylor series expansion out from the wall and is independent of the wall orientation using the expression:

$$\Omega_w=-\frac{\partial^2\Psi}{\partial n^2} \quad (14)$$

where *w* refers to the wall condition and *n* indicates the direction normal to the wall surface.

The finite difference method was used to discretize the governing equations (9) - (11) together with the prescribed boundary conditions. The convective terms of the equations were thereby discretized using the second order upwind difference scheme, which gives better stability and convergence of the computation process and the central differences are used for the diffusive and buoyancy forces. The vorticity transport and energy equations are solved using the Alternating Direction Implicit (ADI) method and the stream function equation is solved by the successive over relaxation method.

The values for the temperature, the stream function, the vorticity, and the velocity components at all the interior grid points were set to zero at the beginning of the computation. The solution algorithm was such that the temperature distribution was foremost determined by solving the energy transport equation. This was followed by the computation of the vorticity and the stream function fields. The wall vorticities were updated from the solution of the stream function equation, while the velocity components are obtained in the dimensionless form from equation (7). The steady state was therefore determined by monitoring the convergence of the temperature and vortex field, using the following convergence criterion.

$$\frac{\sum_{j=2}^{N}\sum_{i=2}^{M}\left|\Phi_{i,j}^{m+1}-\Phi_{i,j}^{m}\right|}{\sum_{j=2}^{N}\sum_{i=2}^{M}\left|\Phi_{i,j}^{m+1}\right|}\le\delta \quad (15)$$

Here the Φ denotes the stream function, Ψ, temperature θ or the vorticity, Ω and m denotes the number of iterations. A value of δ equals 10^{-5} was used in this work which falls between the range of 10^{-3} and 10^{-8} that has been used as stated in different literatures [24].

The local heat flux at steady state is estimated by computing the local Nusselt number on the heated wall:

$$Nu_X=\frac{\dot{Q}_{conv}}{\dot{Q}_{cond}}=-\left(\frac{\partial\theta}{\partial Y}\right)_{Y=0} \quad (16)$$

while the convective heat transfer into the enclosure is evaluated in terms of the average Nusselt number obtained by integrating the local Nusselt number over the entire length of the heated wall:

$$N\overline{u}=\int_0^1 Nu_X\big|_{Y=0}\,dX \quad (17)$$

RESULTS AND DISCUSSIONS

The grid refinement sensitivity of the code used in the present study was carried out by computing the flow

fields with uniform grid systems of 81 x 81, 101 x 101 and 121 x 121 for square enclosures. The results show that the effect of the increase in the grid points above 81 x 81 is insignificant on the flow fields as reflected in our previous work [25]. All computations for the square enclosure in this work were therefore done with a grid system of 81 x 81. The validation of the present code was also done by the comparison of the present results with the published data of Al-Amiri *et al*., [7], Botella and Peyret [26], Bruneav and Jouron [27], Deng *et al*., [28], Ghia *et al*., [29], Barragy and Carey [30], Schreiber and Keller [31] and Khanafer *et al*., [32] as shown in Tables 1 and 2. Table-1 presents the computed values of the maximum horizontal and the vertical velocity components respectively along the vertical and the horizontal mid-plane and the location of their occurrences for mixed forced convection at Reynolds number, $Re = 100$ and Grashof number, $Gr = 100$ in the top lid-driven flow. The maximum absolute stream function is also compared in the table. The maximum absolute stream function and the Nusselt number were also computed for various Reynolds numbers and the results compared with previous works as illustrated in Table-2. The comparison shows a good agreement between the present and the previous results.

Table-1. Comparison of the computed values of the minimum and the maximum velocities components, and the maximum absolute stream function in the enclosure with those of the previous works from Al-Amiri [33], Botella and Peyret [26], Bruneav and Jouron [27], Deng *et al*., [28] and Ghia *et al*., [29] for Reynolds number, $Re = 100$ and $Gr = 100$.

	Present work	**Al-Amiri *et al*.,** [33]	**Botella and Peyret** [26]	**Bruneav and Jouron** [27]	**Deng *et al*.,** [28]	**Ghia *et al*.,** [29]
$\lvert\psi\rvert_{\max}$	0.103336	0.1033	-	-	-	0.103423
$U_{\max}$	0.212672	0.2120	0.21404	0.21315	0.2109	0.2106
$Y_{\max}$	0.4500	0.453	0.4581	-	0.4531	0.4531
$V_{\max}$	0.179421	0.1788	0.17957	0.17896	0.17527	0.1786
$X_{\max}$	0.7667	0.765	0.7630	-	0.7656	0.7656

Table 2. Comparison of the maximum absolute stream function, $\lvert\psi\rvert_{\max}$ and the average Nusselt number, $N\overline{u}$ computed in this work with those from the previous works of Barragy and Carey [30], Schreiber and Keller [31] and Khanafer *et al*., [32] at various Reynolds numbers.

	$\lvert\psi\rvert_{\max}$			$N\overline{u}$	
Re	**Present results**	**Barragy and Carey** [30]	**Schreiber and Keller** [31]	**Present results**	***Khanafer et al.,*** [32]
1	0.100032	0.10005	0.10006	1.00033	-
100	0.103361	0.10330	0.10330	2.03116	2.02
400	0.113596	0.11389	0.11297	4.02462	4.01
500	0.114921	-	-	4.52671	-
1000	0.117890	0.11861	0.11603	6.48423	6.42

The study of the effects of the flow governing parameters on the hydrodynamic and thermal fields and on the heat transfer was conducted by varying the Darcy, Richardson and Péclet number, and the length-to-height aspect ratio respectively in the range $10^{-3} \le Da \le 10$, $0.1 \le Ri \le 10$, $1 \le Pe \le 10^3$ and $0.5 \le AR \le 4$ for a fixed Reynolds number, $Re = 100$. The results are presented in the form of the streamlines and isotherms fields, the dimensionless velocity and temperature profiles, and the heat transfer computed in terms of the local Nusselt number.

Figure-2(a) depicts the hydrodynamic fields in porous medium with Darcy number, $Da = 0.1$ for the cases of pure convection at $Re = 100$, mixed convection at Richardson numbers, $Ri = 1$ and 10, and natural convection for $Ra = 10^5$ all computed for Prandtl number of unity. The fields for the case of the pure convection and that for the mixed convection at $Ri = 1$ are similar and are characterized by two counter cells, indicating that the flow at this Richardson number is characterized by pure forced convection. The results of our numerical simulation show that there is no marked difference in the hydrodynamic fields for $Ri = 0.1$ and 1. The implication is that the mixed convection regime starts at higher value of the Richardson number than the value of $Ri = 0.1$ reported for square enclosure driven on the top-lid [1, 5]. This is to be expected due to the complex configuration being studied here, which is characterized by flow stratification and instability respectively in the lower and upper half of the enclosure. There is an increase in the buoyancy force with

the increase in the Richardson number to $Ri = 10$ resulting in the flow field breaking down to two-cell both on the upper and lower half of the enclosure. The flow field for the case of pure natural convection at $Ra = 10^5$ is presented for comparison purposes. Figure 2b illustrates the corresponding thermal fields for the cases presented in Figure 2a. There is a strong effect of the flow field on the isotherms with the consequence that the isotherms for the pair $Re = 100$ and $Ri = 1$, and for $Ri = 10$ and $Ra = 10^5$ are similar.

The influence of the Richardson and the Darcy number on the flow vigour and on the temperature distribution is quantitatively presented in the form of the velocity and temperature profiles at the vertical mid-plane of the enclosure. The plot of the horizontal velocity at the vertical mid-plane of the square enclosure is presented for various values of the Richardson number for a fixed Darcy number, $Da = 0.1$ in Figure 3a, and for various values of the Darcy number ranging between $Da = 10^{-3}$ and 10 for fixed Richardson number, $Ri = 10$ in Figure 3b. It can be seen from the Figures that the effect of the changes in the Richardson number is stronger in the lower half of the enclosure than in the upper half. The converse is the case for the effect of the changes in the Darcy number on the flow, being stronger in the upper half of the enclosure than in the lower half. This flow pattern is due to the combined effect of the flow configuration and the Darcy and Richardson numbers. While an increase in the Darcy number means more void volume for fluid flow, a decrease in the Darcy number results in the large resistance to the flow circulation. The thermal currents of the flow are suppressed by the porous medium, resulting in a reduction in the overall heat transfer [33]. An increase in the Richardson number leads to the increase in the buoyancy effect which could actually impair or enhance the flow depending on whether it is an aiding or opposing buoyancy force. The temperature profiles at vertical mid-plane of the square enclosure are plotted in Figure 4. The parameter of the curve is the Richardson number for Figure 4a at fixed Darcy number, $Da = 0.1$, and the Darcy number for Figure 4b for fixed Richardson number, $Ri = 10$. Figure 4a shows that the flow activity intensifies as the Richardson number reduces from the value of 10 to 0.01 in the lower half of the enclosure leading to higher heat distribution. This result is in agreement with the result of Al-Amiri [13] for the top-lid driven flow. The Richardson number influences the heat distribution in the upper enclosure in a converse manner to that in the lower enclosure. An increase in the Darcy number from 0.001 to 0.01 results in the increase in the fluid flow and energy transfer. This trend agrees with the results of Oztop [20]. This effect is stronger in the upper enclosure than in the lower enclosure. The curves for $Da = 0.10$ and $Da = 1.0$ collapse to a single curve. This shows that any increase in Darcy number above the value of unity will not bring further gain in the heat transfer. The trend of this result is consistent with what is reported in the literature (i.e., see ref. [33, 34]). The comparison of the effect of the Richardson and Darcy number shows that the effect of the former on the temperature profiles is stronger than that of the latter.

The local Nusselt number computed above and below the moving plate is plotted against the horizontal coordinate. The results are presented in Figures 5 to 8, respectively for various values of Richardson, Darcy and Péclet number, and for different values of the length-to-height aspect ratio. The Figures reveal that for all the cases presented, the local Nusselt number has the highest value at the left side corner of the enclosure due to the temperature discontinuity at this point, and reduces to the lower value at the right side corner of the enclosure. The Darcy number is fixed for $Da = 0.1$ in the results presented in Figure-5. It can be deduced from the figure that the Richardson number has a strong effect on the local Nusselt number. The curves for $Ri = 0.1$ and 1 fall on each other indicating that the reduction in the Richardson number below unity has no effect on the local Nusselt number. The local Nusselt numbers computed above and below the moving plate at the same corresponding point are different due to the difference in the boundary layer effect on both sides of the plate as a result of the different flow configuration. The effect of the Darcy number on the local Nusselt number was also investigated and the results are presented in Figure-6 for a fixed Richardson number, $Ri = 5$. The same trend in the profiles of the local Nusselt number is observed here in comparison with Figure-5. The changes in the Darcy number have stronger effect on the local Nusselt numbers computed above the plate than those determined below it.

Figure-7 is a plot of the local Nusselt number along the moving plate in a square enclosure at fixed Reynolds number, $Re = 100$ and Rayleigh number, $Ra = 10^4$. The curve parameter is the Péclet number, Pe, which is varied between 1 and 10^3. Increasing the Péclet number between the value of unity and 10 only affect the local Nusselt number slightly. Further increase in the values of the Péclet number between $Pe = 10^2$ and 10^3 results in an appreciable increase in the local Nusselt number in agreement with the earlier results presented by Waheed [35] and, Moallemi and Jang [36]. Finally, the effect of the aspect ratio on the local Nusselt number was investigated. The results presented in Figure 8 show that an increase in the aspect ratio leads to a decrease in the local Nusselt number in agreement with the results presented by Corcione [37].

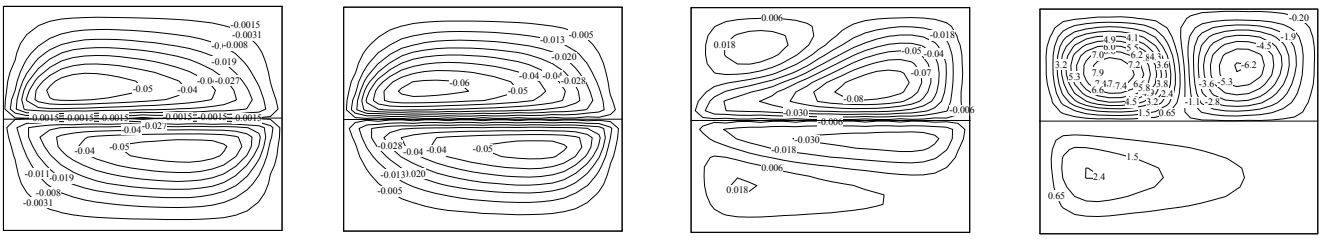

(i) $Re = 100$ (ii) $Ri = 1.0$ (iii) $Ri = 10$ (iv) $Ra = 10^5$

Figure-2(a).

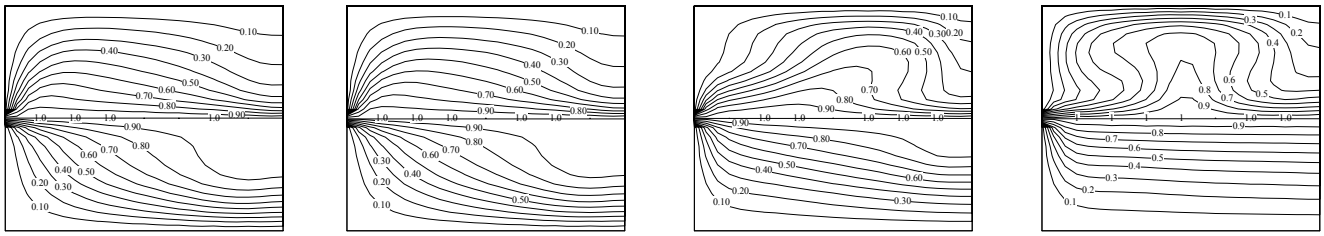

(i) $Re = 100$ (ii) $Ri = 1.0$ (iii) $Ri = 10$ (iv) $Ra = 10^5$

Figure-2(b).

Figure-2. (a) The hydrodynamic and (b) temperature fields for (i) forced convection, $Re = 100$, (ii) mixed convection, $Ri = 1.0$, (iii) mixed convection, $Ri = 10$, and (iv) natural convection, $Ra = 10^5$ in the square enclosures at $Da = 0.1$.

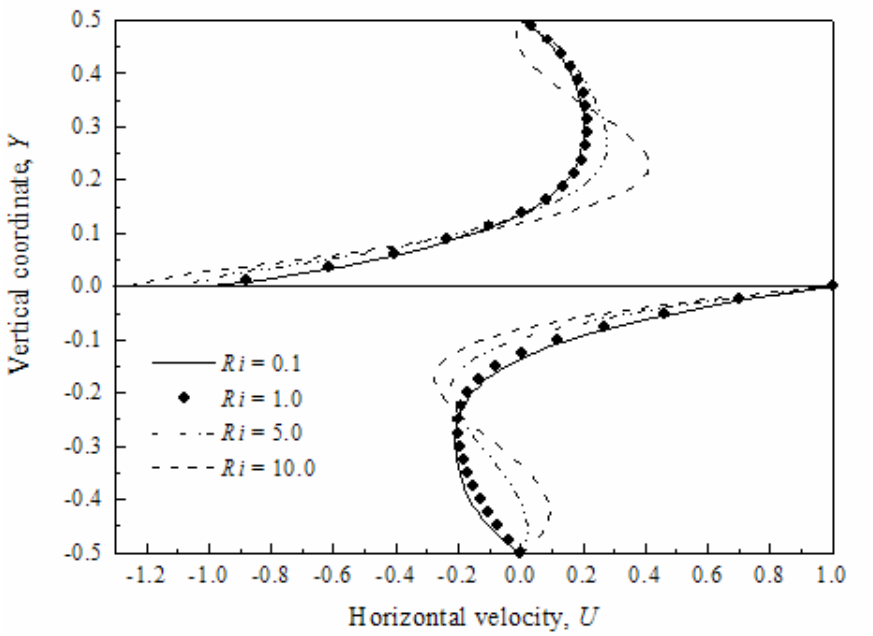

Figure-3(a).

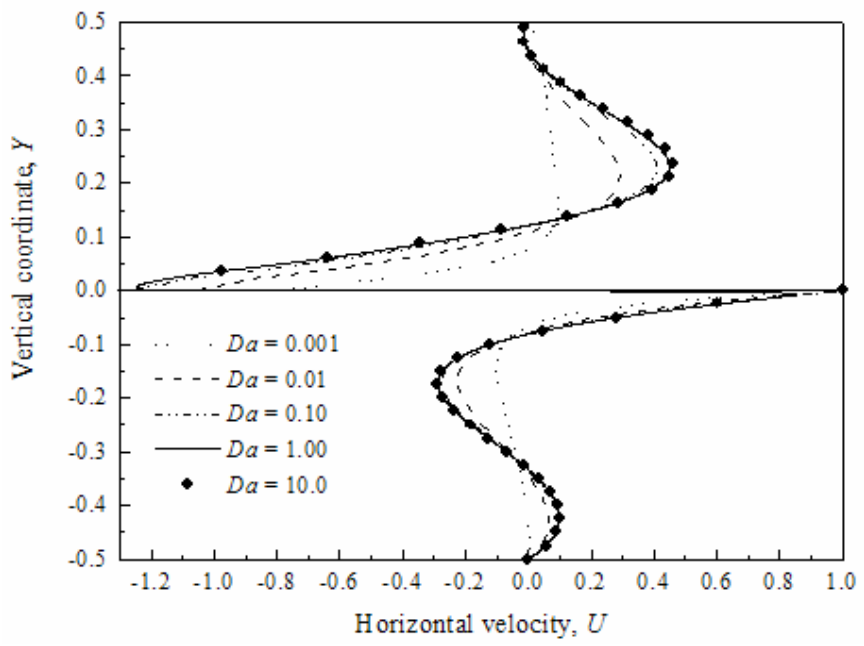

Figure-3(b).

Figure-3. The horizontal velocity profiles across the vertical mid-plane, for Re = 100, Pr = 1 and AR = 1 (a) for various Richardson numbers and fixed Da = 0.1, and (b) for different Darcy numbers and fixed Ri = 10.

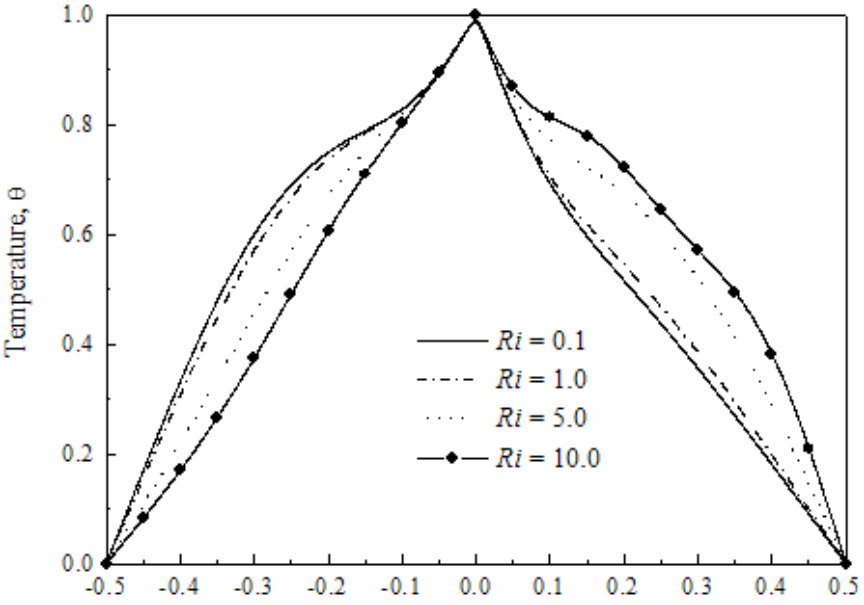

Figure-4(a).

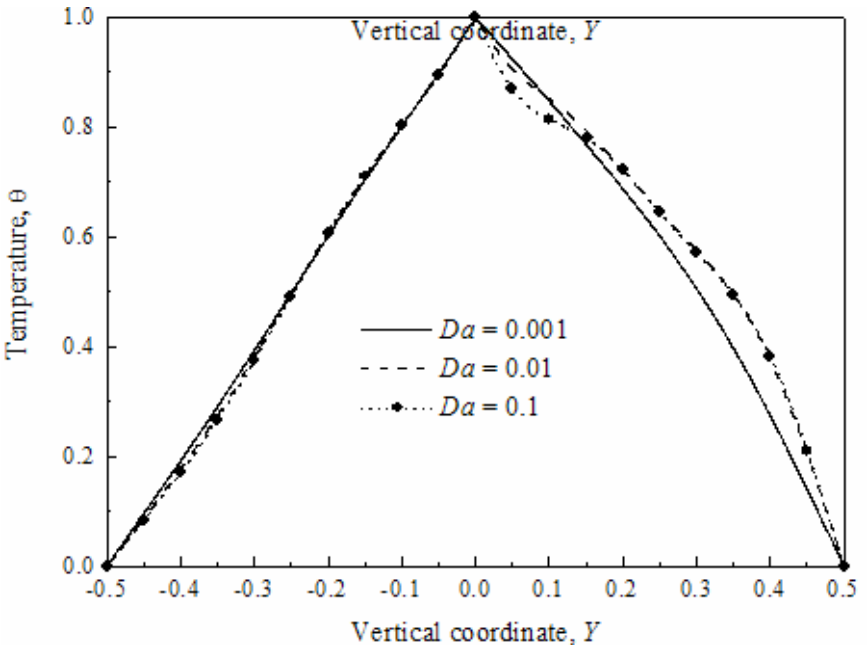

Figure-4(b).

Figure-4. The temperature profiles across the vertical mid-plane, for Re = 100, Pr = 1 and AR = 1 (a) for various Richardson numbers and fixed Da = 0.1, and (b) various Darcy numbers and fixed Ri = 10.

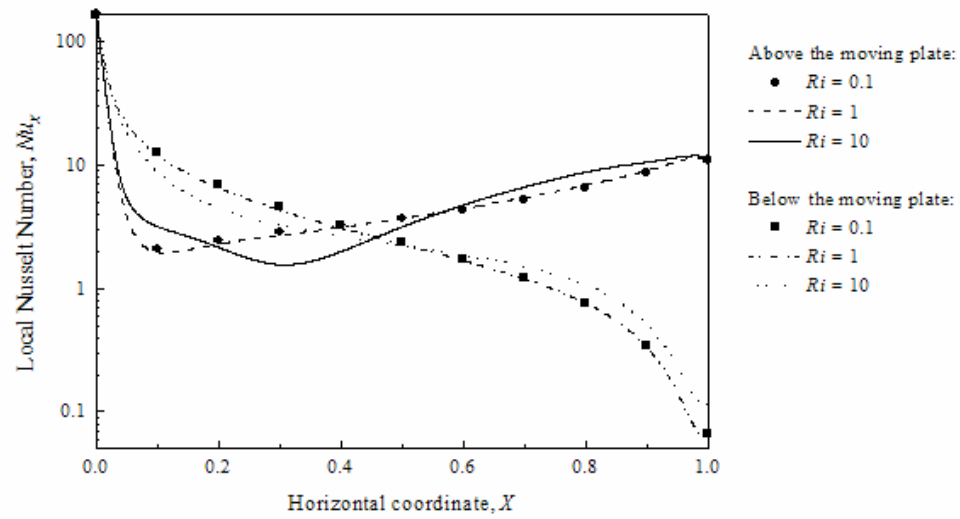

Figure-5. The effects of the Richardson number, Ri, on the local Nusselt number along the horizontal heated wall for Re = 100, Pr = 0.71, Da = 0.1 and AR = 1.

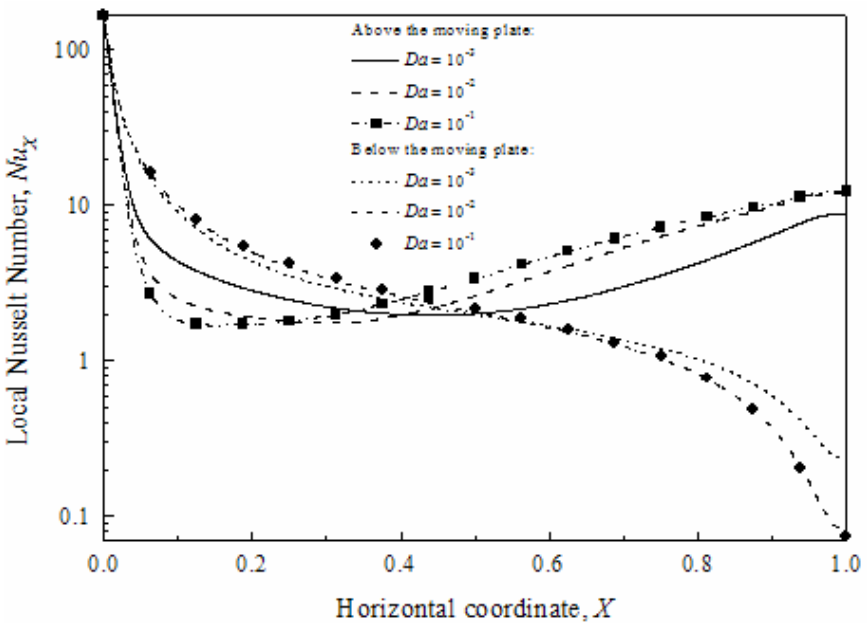

Figure-6. The effects of the Darcy number, *Da*, on the local Nusselt number along the horizontal heated wall for *Ri* = 5.0, *Re* = 100, *Pr* = 1 and *AR* = 1.

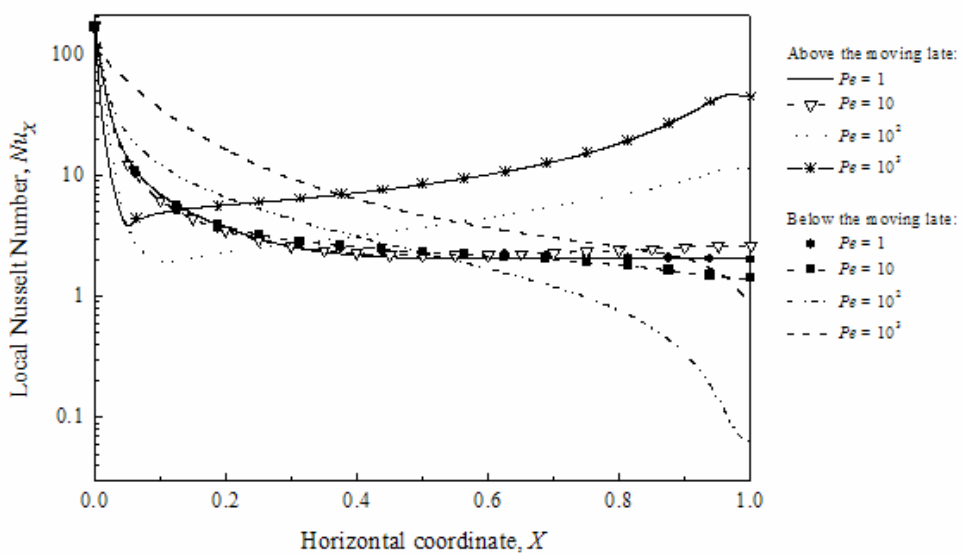

Figure-7. The effects of the Péclet number, *Pe*, on the local Nusselt number along the horizontal heated wall *Re* = 100, *Ra* = 10^4, *Da* = 0.1 and *AR* = 1.

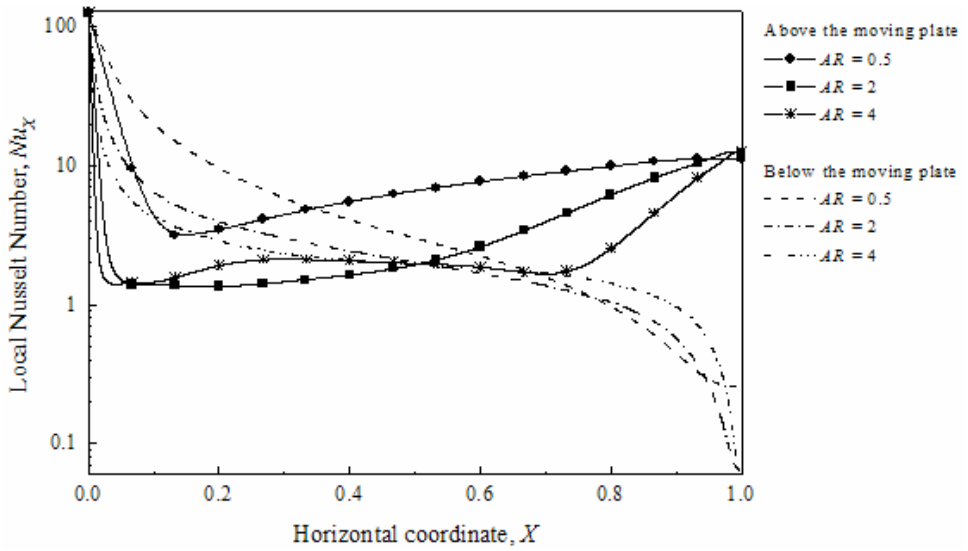

Figure-8. The effects of the aspect ratio, *AR*, on the local Nusselt number along the horizontal heated wall for *Ri* = 5.0, *Re* = 100, *Pr* = 1 and *Da* = 0.1.

Nomenclature

AR	-	Length-to-height aspect ratio (= *L*/*H*)
c_p	-	Specific heat capacity of fluid
Da	-	Darcy number, (= K/H^2)
g	-	Acceleration due to gravity
Gr	-	Grashof number, (= $g\beta(T_w - T_c)H^3/\nu^2$)
H	-	Height of the enclosure
h	-	Heat transfer coefficient
k	-	Fluid thermal conductivity
K	-	Permeability
L	-	Length of the enclosure
M	-	Number of horizontal grid lines
N	-	Number of vertical grid lines
n	-	Normal direction to wall
Nu	-	Average Nusselt number, (= $\dot{Q}/k\Delta T = hL/k$)
Nu_x	-	Local Nusselt number
p	-	Pressure
Pe	-	Péclet number, (= $\mathrm{Pr}\,\mathrm{Re} = U_w H/\alpha$)
Pr	-	Prandtl number, (= ν /α)
$\dot{Q}$	-	Overall heat transfer rate
Ra	-	Rayleigh number, (= $\mathrm{GrPr} = g\beta(T_w - T_c)H^3/\alpha\nu$)
Re	-	Reynolds number, (= $U_w H$/ν)
Ri	-	Richardson number, (= $Gr/\mathrm{Re}^2 = g\beta(T_w - T_c)H/U_w^2$)
T	-	Temperature
t	-	Time
u	-	Velocity vector
U	-	Dimensionless velocity vector
u	-	Horizontal velocity component
U	-	Dimensionless horizontal velocity component
v	-	Vertical velocity component
V	-	Dimensionless vertical velocity component
x	-	Horizontal coordinate
X	-	Dimensionless horizontal coordinate
y	-	Vertical coordinate

Y - Dimensionless vertical coordinate

Greek alphabet

α - Fluid thermal diffusivity, ($\alpha = k/\rho c_p$)
β - Volumetric coefficient of thermal expansion
δ - Residual value
μ - Viscosity
ν - Kinematic viscosity
θ - Dimensionless temperature, $(T - T_c)/(T_w - T_c)$
ρ - Density
τ - Dimensionless time
ω - Vorticity
Ω - Dimensionless vorticity
ψ - Stream function
Ψ - Dimensionless Stream function

Sub- and superscripts

c - Condition of ambient medium
e - Effective
f - Fluid
m - Number of iterations
s - Solid
w - Condition of moving wall

CONCLUSIONS

The buoyancy- and the shear-driven flow induced by a hot plate moving through the horizontal mid-plane of a rectangular enclosure filled with fluid-saturated porous medium has been studied numerically in this work. One of the enclosure's external vertical walls is thermally isolated while all the other walls are at ambient temperature. The continuity, the generalised Darcy-Brinkman-Forchheimer extended momentum, and the energy transport equations were solved using the finite difference technique. The results generated in the work were validated with the available data in the literature and the agreements with the previous results were good. The results had been presented in the form of the hydrodynamic and thermal fields, and the profiles for velocity, temperature and local Nusselt number. The results show strong dependence of the heat distribution and the fluid circulation within the enclosure on the flow governing parameters including the Richardson, Darcy and Péclet numbers, and the length-to-height aspect ratio. Due to the complex boundary condition occasioned by the position of the moving plate, the flow above and below it is characterised by instability and stratification respectively. Consequently, different rate of heat transfer is obtained at the same coordinate point on both sides of the plate for some flow parameters. The designer of heat transfer equipment with this kind of flow geometry must therefore put this factor into consideration to achieve results that will improve and optimize the performance in practical applications.

REFERENCES

[1] O. Aydin. 1999. Aiding and opposing mechanisms of mixed convection in a shear- and buoyancy-driven cavity, Int. Commun. Heat and Mass Transfer. 26(7): 1019-1028.

[2] N. Allborn, H. Raszillier, F. Durst. 1999. Lid-driven cavity with heat and mass transport. Int. J. Heat Mass Transfer. 42: 833-853.

[3] Y. Jaluria. 2001. Fluid flow phenomena in materials processing - the 2000 Freeman 502 Scholar Lecture. ASME J. Fluids Eng. 123: 173-210.

[4] M.A.R. Sharif. 2007. Laminar mixed convection in shallow inclined driven cavities with hot moving lid on top and cooled from bottom. Appl. Therm. Eng. 27(505): 1036-1042.

[5] J.C.F. Wong. 2007. Numerical simulation of two-dimensional laminar mixed-convection in a lid-driven cavity using the mixed finite element consistent splitting scheme. Int. J. Numer. Methods Heat Fluid Flow. 17(1): 46-93.

[6] W. -J. Luo, R.-J. Yang. 2007. Multiple fluid flow and heat transfer solutions in a two-sided lid-driven cavity. Int. J. Heat Mass Transfer. 50: 2394-2405.

[7] A.M. Al-Amiri, K.M. Khanafer, I. Pop. 2007. Numerical simulation of combined thermal and mass transport in a square lid-driven cavity. Int. J. Therm. Sci. 46: 662-671.

[8] G. Degan, P. Vasseur. 1997. Boundary-layer regime in a vertical porous layer with anisotropic permeability and boundary effects. Int. J. Heat Fluid Flow 18: 334-343.

[9] R. Bennacer, H. Beji, A.A. Mohamad. 2003. Double diffusive convection in a vertical enclosure inserted with two saturated porous layers confining a fluid layer. Int. J. Therm. Sci. 42: 141-151.

[10] A. C. Baytaş. 2003. Thermal non-equilibrium natural convection in a square enclosure filled with a heat generating solid phase, non-Darcy porous medium. Int. J. Energy Res. 27: 975-988.

[11] D.A.S. Rees, A.P. Bassom, P.G. Siddheshwar. 2008. Local thermal non-equilibrium effects arising from the injection of a hot fluid into a porous medium. J. Fluid Mech. 594: 379-398.

[12] A.C. Baytas, I. Pop. 2002. Free convection in a square porous cavity using a thermal nonequilibrium model. Int. J. Therm. Sci. 41: 861-870.

[13] A.M. Al-Amiri. 2000. Analysis of momentum and energy transfer in a lid-driven cavity filled with a porous medium. Int. J. Heat Mass Transfer. 43: 3513-3527.

[14] K. Khanafer, K. Vafai. 2002. Double-diffusive mixed convection in a lid-driven enclosure filled with a fluid-saturated porous medium. Numer. Heat Transfer A. 42: 465-486.

[15] K.M. Khanafer, A.J. Chamkha. 1999. Mixed convection flow in a lid-driven enclosure filled with a fluid-saturated porous medium. Int. J. Heat Mass Transfer. 42: 2465-2481.

[16] D.A. Nield, A. Bejan. 2006. Convection in porous media. 3rd edition, Springer Verlag, New York, USA.

[17] E. Holzbecher, Y. Yusa. 1995. Numerical experiments on free and forced convection in porous media. Int. J. Heat Mass Transfer. 38(11): 2109-2115.

[18] M.M. Abdelkhalek. 2008. Mixed convection in a square cavity by a perturbation technique. Comput. Mater. Sci. 42: 212-219.

[19] T.C. Jue. 2002. Analysis of flows driven by a torsionally-oscillatory lid in a fluid-saturated porous enclosure with thermal stable stratification. Int. J. Therm. Sci. 41: 795-804.

[20] H.F. Oztop. 2006. Combined convection heat transfer in a porous lid-driven enclosure due to heater with finite length, Int. Comm. Heat Mass Transfer. 33: 772-779.

[21] V.A.F. Costa, L.A. Oliveira, B.R. Baliga, A.C.M. Sousa. 2004. Simulation of coupled flows in adjacent porous and open domains using a control-volume finite-element method. Numer. Heat Transfer A. 45: 675-697.

[22] J.L. Lage. 1998. The fundamental theory of flow through permeable media from Darcy to turbulence: in Transport Phenomena in Porous Media edited by D. B. Ingham and I. Pop, Elsevier Science Ltd. pp. 1- 30.

[23] S. Ergün. 1952. Fluid flow through packed columns, Chem. Eng. Progress. 48: 89-94.

[24] T.J. Chung. 2002. Computational Fluid Dynamics. Cambridge University Press, Cambridge, U.K.

[25] M.A. Waheed. 2009. Mixed convective heat transfer in rectangular enclosures driven by a continuously moving horizontal plate. Int. J. Heat Mass Transfer (2009), doi:10.1016/j.ijheatmasstransfer. 05.011

[26] O. Botella, R. Peyret. 1998. Benchmark spectral results on the lid-driven cavity flow. Comput. Fluids. 27: 421-433.

[27] C.-H. Bruneau, C. Jouron. 1990. An efficient scheme for solving steady incompressible Navier-Stokes equations. J. Comput. Phys. 89: 389-413.

[28] G.B. Deng, J. Piquet, P. Queutey, M. Visonneau. 1994. Incompressible flow calculations with a consistent physical interpolation finite volume approach. Comput. Fluids. 23: 1029-1047.

[29] U. Ghia, K.N. Ghia, C.T. Shin. 1982. High-*Re* solutions for incompressible flow using the Navier–Stokes equations and a multigrid method. J. Comput. Phys. 48: 387-411.

[30] E. Barragy, G.F. Carey. 1997. Stream function-vorticity driven cavity solution using p finite elements. Comput. Fluids. 26(5): 453-468.

[31] R. Schreiber, H.B. Keller. 1983. Driven cavity flows by efficient numerical techniques, J. Comput. Phys. 49: 310-333.

[32] K.M. Khanafer, A.M. Al-Amiri, I. Pop. 2007. Numerical simulation of unsteady mixed convection

in a driven cavity, using an externally excited sliding lid, Eur. J. Mech. B Fluids. 26: 669-687.

[33] A.M. Al-Amiri. 2002. Natural convection in porous enclosures: The application of the two-energy equation model. Numer. Heat Transfer A. 41(8): 817-834.

[34] M.A. Waheed. 2009. Heatfunction formulation of thermal convection in rectangular enclosures filled with porous media. Numer. Heat Transfer A. 55(2): 185-204.

[35] M.A. Waheed. 2006. Temperature dependent fluid properties effect on the heat function formulation of natural convective flow and heat transfer. Int. J. Numer. Methods Heat Fluid Flow. 16(2): 240-257.

[36] M.K. Moallemi, K.S. Jang. 1992. Prandtl number effects on laminar mixed convection heat transfer in a lid-driven cavity. Int. J. Heat Mass Transfer. 35: 1881-1892.

[37] M. Corcione. 2003. Effects of the thermal boundary conditions at the sidewalls upon natural convection in rectangular enclosures heated from below and cooled from above. Int. J. Therm. Sci. 42: 199-208.